Int J Adv Manuf Technol (1997) 13:738–746

The International Journal of
Advanced Manufacturing Technology

Implementation of a Kalman Filter in Positioning for Autonomous Vehicles, and its Sensitivity to the Process Parameters

S. Shoval, I. Zeitoun and E. Lenz

Technion–Israel Institute of Technology, Haifa, Israel, Center for Manufacturing Systems and Robotics, Department of Mechanical Engineering, Haifa, Israel

Modern autonomous vehicles are using more than one method for performing the positioning task. The most common positioning methods for indoor vehicles are odometry for relative positioning and triangulation for absolute positioning. In many cases a Kalman filter is required to merge the data from the positioning systems and determines the vehicle position based on error analysis of the measurements and calculation procedures. A Kalman filter is particularly advantageous for "on-the-fly" positioning, which is performed while the vehicle is in motion. This paper presents the implementation of a Kalman filter in "ROBI" – an AGV for material handling in a manufacturing environment. The performance of the filter in estimating the position of the AGV and the effect of motion parameters (speed, path curvature, beacon layout etc.) on filter accuracy are shown.

Keywords: AGV; Kalman filter; Positioning; Process parameters

1. Introduction

Various types of positioning method are used by Automated Guided Vehicles (AGVs). Selection of a particular method is based on the type of sensory data, the required application, and the environment in which the vehicle is operating.

Rigid navigation systems guide the vehicle along a predefined tracks with limited flexibility. Among the common rigid methods are the mechanical track (similar to train tracks), electric/magnetic systems which guide the vehicle by a wire laid under the floor, optic/chemical strips which are laid on the floor surface, and the Binary-Pseudo-Random method that guides the vehicle by a coded wire [1].

Free range positioning systems provide flexible guidance of autonomous vehicles. Such systems are advantageous for vehicles operating in unstructured or unknown environments, and enable the implementation of complicated tasks such as obstacle avoidance, path planning, reactive motion, etc. Several systems are used for free range navigation.

Odometry. Vehicle position is determined by geometric interpolation according to the angular displacement of the vehicle's wheels. This method provides only incremental positioning, and has, therefore, limited accuracy, especially as the distance travelled increases. It is sensitive to external disturbances (slippage, uneven surfaces, etc.) and internal disturbances (unbalanced wheels, encoder/resolver resolution, etc.), but does not require initial set-up of the environment. Many commercial mobile robots and AGVs are using odometry (A2k [2], Denning [3], Nomad [4]) either as a primary or a secondary positioning system.

Beacon Based Navigation. Vehicle position is determined by relative measurements of the vehicle to predefined landmarks (beacons), the locations of which are known. Measurement can consist of angular or linear data, and can be performed by laser transmitter/receiver, infra-red systems, ultrasonic sensors, vision, satellites, etc. One system of landmark navigation uses angular measurements for triangulation. Other systems use linear measurements for positioning, usually by measuring the time-of-flight of ultrasonic waves.

Inertial Navigation Systems. Vehicle position is determined by accelerometers and/or gyroscopes which measure the vehicle's linear and angular motions. Fujiwara et al. [5] and Nakano et al. [6] describe a mobile robot using a gyroscope and optical encoders for navigation among several assembly stations. Barshan and Durrant-Whyte [7] developed a navigation system for mobile robots based on a gyroscope and accelerometer.

Estimation of vehicle position often requires data fusion of several sensors, using different positioning methods. In many applications, the vehicle is using Odometry (for relative positioning) with additional sensors. Ishikawa and Sampei investigate three methods for data fusion in position estimation of autonomous vehicles:

1. Direct Liaponov method [8,9]
2. Nonlinear Lowenberger estimation [10]
3. Nonlinear Kalman filter [11]

Correspondence and offprint requests to: E. Lenz, Technion – Israel Institute of Technology, Center for Manufacturing Systems and Robotics, Department of Mechanical Engineering, Haifa 32000, Israel.

Bar-Shalom and Fortman [12], and Smith et al. [13] describe the extended Kalman filter. Leonard and Durrant-Whyte [14] use data fusion of odometry and ultrasonic sensors with geometric beacons for positioning of mobile robots. Von der Hardt et al. [15] apply a Kalman filter in the ROMANE mobile robot which uses a magnetometer data and odometry. A similar method is used by Kriegman et al. [16] in their SRI mobile robot which is equipped with a stereo vision system for navigation inside buildings. Stella et al. [17] describe a position estimation technique based on data fusion obtained from two independent subsystems: an onboard camera using artificial landmarks, and a dead reckoning subsystem using odometry. A similar system was used by CARMEL – the University of Michigan's winning entry in the AAAI-92 Autonomous Robot Competition [18]. Several systems use a rotating laser beam which measures the angular position of the vehicle to retro-reflectors [19–22].

Cicci [23] describes an adaptive extended Kalman filter to improve the accuracy in position estimation of a target in tracking/intercept problems. The adaptive filter is used to reduce the effect of poor observability due to closing geometries. Shoval et al. [22] analyse errors in position estimation using geometric triangulation, due to closing beacons geometry.

In this paper we present a positioning system for a mobile robot using data fusion of odometry, and a rotating laser beam with retro-reflectors. In particular we discuss the effects of the sensitivity of the extended Kalman filter to various parameters involved in the travel process. The positioning system is implemented and tested in ROBI – a mobile robot operating in an industrial environment. The robot is operating in a flexible manufacturing system (FMS) for material and tool handling. The system includes two CNC cells with robots for loading and unloading, two robotic assembly stations, an inspection and quality control station, and a linear uni-directional conveyor for material transfer. Each of the CNC cells and the conveyor have docking points for interface with the AGV.

2. The Mobile Robot – ROBI

Figure 1 describes the robot's general structure. The driving unit is of an asynchronous type and consists of two stepping motors. In addition, the robot is equipped with four castor wheels for stability. Each motor is driven by a separate controller which provides the required pulse frequency. The linear velocity of each wheel is given by equation (1).

$$V_{\text{left}} = \frac{2\pi R_{\text{left}} n_{\text{left}}}{NT} \tag{1a}$$

$$V_{\text{right}} = \frac{2\pi R_{\text{right}} n_{\text{right}}}{NT} \tag{1b}$$

where R_{left} and R_{right} are the radii of the right and left wheels, T is the gear ratio from the driving motor to the wheels, N is the motor resolution (pulse per revolution), and n_{left} and n_{right} are the pulse frequencies for the left and right wheels.

The measurement unit (Fig. 2) consists of a rotating low-power laser system. The system continuously transmits a narrow beam parallel to the floor plane. Several reflectors are

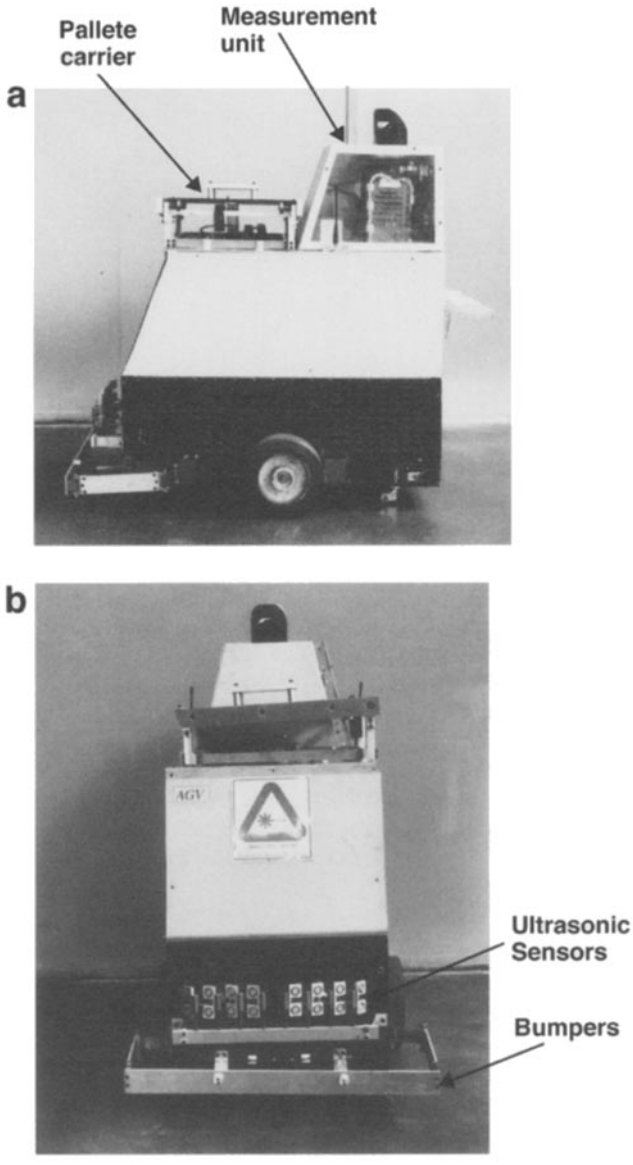

Fig. 1. General structure of ROBI. (*a*) Side view. (*b*) Front view.

located in predefined locations in the working area, to reflect the laser beam back to an optical detector on the robot. The angular position of the rotating unit is measured by an optical encoder, which records the position as soon as the optical sensor detects a reflected beam. A series of optical lances and mirrors focuses the transmitted and reflected laser beams to the required wavelength. The unit rotates at 3 Hz and can reliably detect reflectors located up to 10 m (30 ft) from the vehicle. The system resolution is 1.7×10^{-3} rad (0.1°). The reflectors are 500 m long, with a square profile (15 × 15 mm). Theoretically, a circular profile is preferable, but such a profile reduces the bandwidth of the reflectors, and reduces the effective distance to 3 m (10 ft) only.

Figure 3 shows the vehicle entering one of the docking stations of the conveyor. For the loading task, the lift is raised before the AGV enters the port. Once it is positioned accu-

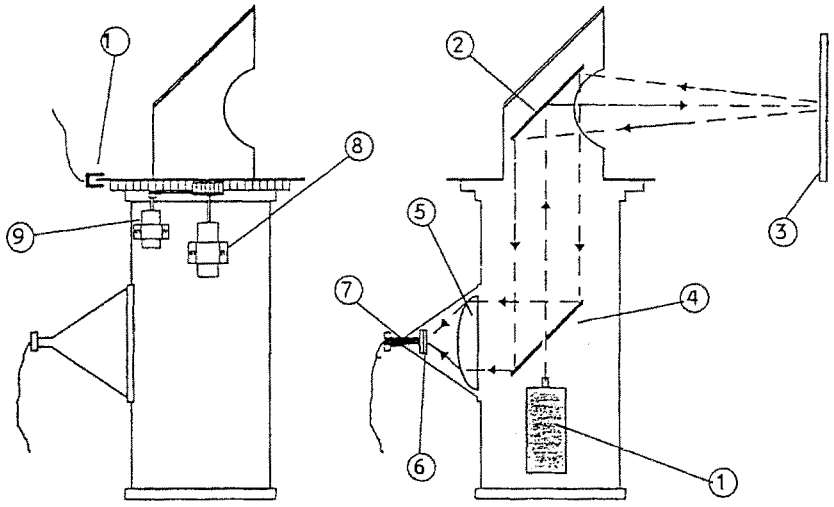

Fig. 2. The measuring unit. 1. Laser transmitter. 2. Rotating mirror. 3. Reflector. 4. Stationary mirror. 5. Lens. 6. Optical filter. 7. Optical sensor. 8. d.c. Motor. 9. Encoder. 10. Calibration sensor.

rately, the lift is lowered, and the pallet is pulled by the conveyor. For unloading, the process is reversed, and the AGV enters the port with the lift in its lower position. After the vehicle is positioned, the lift picks up the pallet and the vehicle leaves the port.

The robot is equipped with mechanical bumpers which cut the power to the driving motors in the event of a collision. It also has ultrasonic sensors for obstacle detection and avoidance, communication antennas and a control/interface panel.

3. Position Estimation with a Kalman Filter

Two sources of information are available for position estimation:

1. Odometry.
2. Triangulation.

None of these methods are sufficient for accurate and reliable estimation of the vehicle position. Odometry can determine only the relative position and accumulates errors as the distance travelled increases. Triangulation can provide reliable information while the vehicle is stationary, but produces an erroneous position estimate when performed during motion. A better estimate is, therefore, obtained by data fusion. Figure 4 shows a block diagram for the Kalman filter in data fusion of odometry and angular measurement to beacons. The following denotes the filter parameters:

$\mathbf{X}(k) = (x_k, y_k, \theta_k)^T$, robot pose (lateral position – x, y and orientation θ_k) at discrete time k.

γ_j, measurement to the jth landmark.

$\hat{\mathbf{X}}(k+1|k)$, prediction of robot pose at discrete time $(k+1)$ based on pose at k.

$\tilde{\gamma}_j(k+1|k)$, prediction of angular measurement to jth reflector at discrete time $(k+1)$ based on pose at k.

$\hat{\mathbf{X}}(k+1|k+1)$, estimate of robot pose at discrete time $(k+1)$.

The Kalman filter consists of the modules described in Sections 3.1 and 3.2.

3.1 State Prediction

The state prediction is based on the robot motion model (process model). Define an input vector $\mathbf{u}_k$ as

$$\mathbf{u}_k = \begin{pmatrix} \delta d_k \\ \delta\theta_k \end{pmatrix} \tag{2}$$

where

$$\delta d_k = v_k T s \tag{3a}$$

and

$$\delta\theta_k = \frac{v_k}{\rho_k} T s \tag{3b}$$

T_s is the sampling rate, V_k the linear velocity of the robot centre and ρ_k is the momentary radius of curvature of the vehicle path. V_k and ρ_k are given by

$$V_k = \frac{V_{\text{left}} + V_{\text{right}}}{2} \tag{3c}$$

$$\rho_k = \frac{D(V_{\text{right}} + V_{\text{left}})}{2(V_{\text{right}} - V_{\text{left}})} \tag{3d}$$

where V_{left} and V_{right} are determined by equations $(1a)$ and $(1b)$. D is the distance between the two driving wheels.

Defining the vectoric function $f(\hat{\mathbf{X}}(k|k), \mathbf{u}_k)$ for the odometry model, von der Hardt et al. [15] show that, for small angles, f is given by:

$$\mathbf{x}_{k+1} = \mathbf{x}_k + \mathbf{u}_k(1) \cos(\theta_k + \tfrac{1}{2}(\mathbf{u}_k(2)) \tag{4a}$$

$$y_{k+1} = y_k + \mathbf{u}_k(1) \sin(\theta_k + \tfrac{1}{2}(\mathbf{u}_k(2)) \tag{4b}$$

$$\theta_{k+1} = \theta_k + \mathbf{u}_k(2) \tag{4c}$$

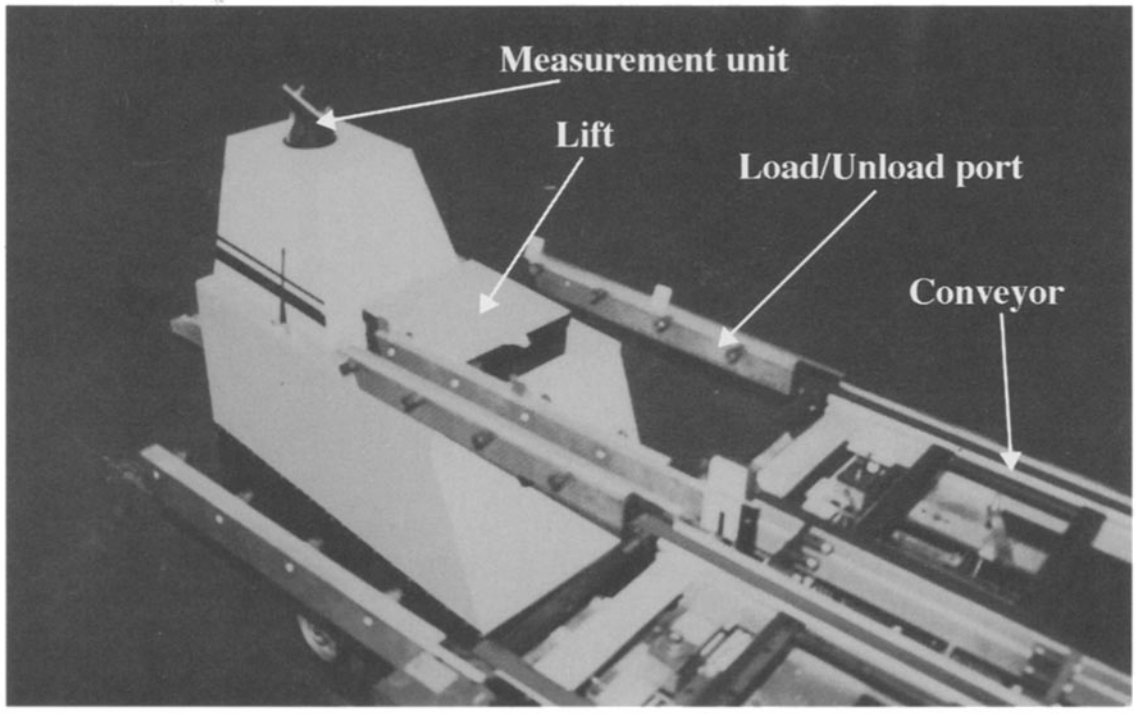

Fig. 3. The vehicle entering one of the docking stations of the conveyor.

3.2 Measurement Prediction

Given the robot state at discrete time $(k+1)$, $\mathbf{X}_{k+1} = (x_{k+1}, y_{k+1}, \vartheta_{k+1})^T$, the measurement γ_j is the angle between the directional vector of the robot $\mathbf{u}$ (unit vector) and the reflected beam vector $\mathbf{t}$ (Fig. 5). The reflected beam vector $\mathbf{t}$ is the vectoric difference between the beacon vector $\mathbf{R}_j$ and the vector pointing to the centre of the laser transmitter/receiver $\mathbf{r}$. The measurement parameters are therefore given by:

$$\mathbf{u} = (\cos\theta_{k+1}, \sin\theta_{k+1})^T \tag{5}$$

$$|\gamma_j| = a\cos\left(\frac{\mathbf{u}\cdot\mathbf{t}}{|\mathbf{u}|\cdot|\mathbf{t}|}\right) \tag{6}$$

$$|\gamma_j| = a\sin\left(\frac{|\mathbf{u}\times\mathbf{t}|}{|\mathbf{u}|\cdot|\mathbf{t}|}\right) \tag{7}$$

$$\gamma_j = a\tan2(|\mathbf{u}\times\mathbf{t}|, \mathbf{u}.\mathbf{t}) \tag{8}$$

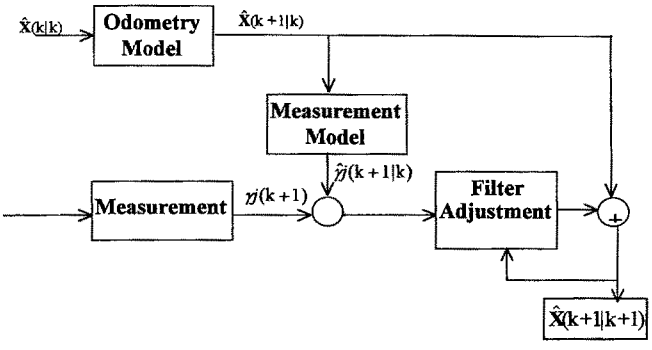

Fig. 4. Block diagram of the Kalman filter.

$$\mathbf{t} = \mathbf{R}_j - \mathbf{r} \tag{9}$$

and finally

$$\gamma_j = a\tan2(|\mathbf{u}x(R_j - \mathbf{r})|, \mathbf{u}.(\mathbf{R}_j - \mathbf{r})) \tag{10}$$

If the laser unit is offset from the robot centre (the centre between the two wheels) $\mathbf{r}$ is determined by

$$\mathbf{r} = \mathbf{X}' + \mathbf{c} \tag{11}$$

where $\mathbf{X}' = (x_{k+1}, y_{k+1})^T$ and $\mathbf{c} = -L\mathbf{u}$.

L is the offset (in length unit) of the laser unit from the vehicle centre (Fig. 6).

The measuring function is, therefore, expressed as

$$\hat{\gamma}_j(k+1|k) = a\tan2(|\mathbf{u}x(\mathbf{R}_j - \mathbf{X}')|, \mathbf{u}.(\mathbf{R}_j - \mathbf{X}') + L) \tag{12}$$

or

$$\hat{\gamma}_j(k+1|k) = h_j(\hat{\mathbf{X}}(k+1|k)) \tag{13}$$

3.3 Determination of the Kalman Filter's Gains

Determination of the filter's gains is determined by a statistical analysis of the models and measurements involved in the process. These analyses provide the covariance matrices which determine the filter's gains.

First, considering the odometry model, there are several sources for errors:

Slippage of wheels (single or both).

Uneven floor surface.

Uncertainties in mechanical parameters (distance between wheels, wheels' diameter, wheels' alignment, contact point between the wheel and the floor).

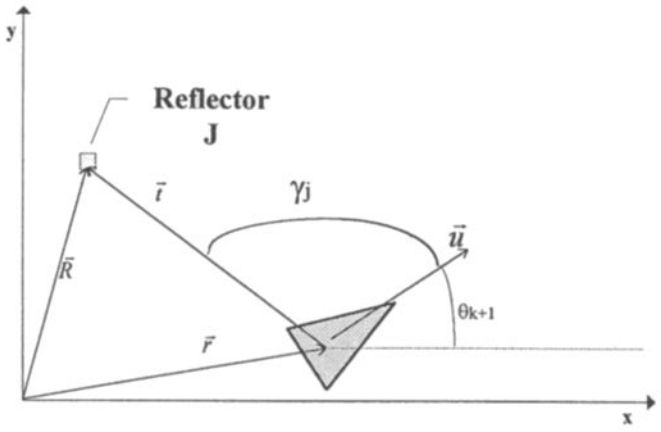

Fig. 5.

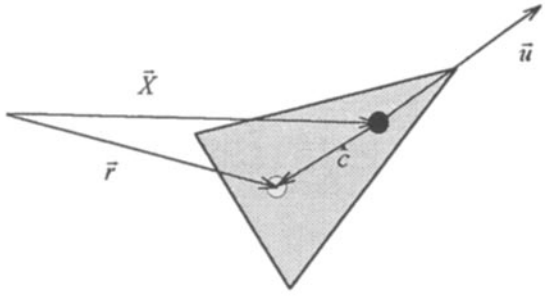

Fig. 6. ▨, laser centre; ■, vehicle centre.

Numerical errors in the geometric calculations.

Adding a random error (W_r and W_l) to each wheel produces:

$$\delta \mathrm{d}r = 2\pi\omega_r T_S R_{\text{right}} + W_r \tag{14a}$$

$$\delta \mathrm{d}l = 2\pi\omega_l T_S R_{\text{left}} + W_l \tag{14b}$$

where R_{right} and R_{left} are the radii of the wheels, and ω_r and ω_l are the angular speeds of the wheels. Moutarlier and Chatila [24] suggest modelling W_r and W_l as independent white noise with variance σr^2 and σl^2, where

$$\sigma r^2 = (\alpha \delta \mathrm{d}r)^2 \tag{15a}$$

$$\sigma l^2 = (\sigma \delta \mathrm{d}l)^2 \tag{15b}$$

In this model, α is determined by experiment.

Defining $\mathbf{u}_k^*$ as a new input vector (which also includes the error)

$$\mathbf{u}_k^* = (\delta \mathrm{d}_k^*, \delta\theta_k^*)^T \tag{16}$$

where δd_k^* and $\delta\theta_k^*$ are the actual angular and lateral displacements (including the error) and are given by

$$\delta d_k^* = \frac{\delta \mathrm{d}r + \delta \mathrm{d}l}{2} \tag{17a}$$

$$\delta\theta_k^* = \frac{\delta \mathrm{d}r - \delta \mathrm{d}l}{D} \tag{17b}$$

where D is the distance between the driving wheels.

Combining equations (12) and (15) produces

$$\delta d_k^* = \pi T_S R(\omega r + \omega l) + \frac{W_r + W_l}{2} \tag{18a}$$

$$\delta\theta_k^* = \frac{2\pi T_S R(\omega r - \omega l)}{D} + \frac{W_r - W_l}{D} \tag{18b}$$

and

$$\delta d_k^* = \delta d_k + \frac{W_r + W_l}{2} \tag{19a}$$

$$\delta d_k^* = \delta\theta_k + \frac{W_r - W_l}{D} \tag{19b}$$

Now, u_k^* can be expressed as

$$\mathbf{u}_k^* = \mathbf{u}_k + \begin{bmatrix} 1/2 & 1/2 \\ 1/D & -1/D \end{bmatrix} \mathbf{W} \tag{20}$$

where $\mathbf{W} = (W_r, W_l)^T$.

The Odometry model can, therefore, be expressed by

$$\mathbf{X}(k+1) = f(\mathbf{X}(k), \mathbf{u}_k) + G_k \mathbf{W} \tag{22}$$

where f is the vectoric function shown in equation (4), and G_k is the coefficient matrix to the error vector, given by

$$G_k = \frac{1}{2} \begin{bmatrix} \cos\left(\theta_k + \frac{u_k(2)}{2}\right) - \frac{u_k(1)}{D}\sin\left(\theta_k + \frac{u_k(2)}{2}\right) & \cos\left(\theta_k + \frac{u_k(2)}{2}\right) + \frac{u_k(1)}{D}\sin\left(\theta_k + \frac{u_k(2)}{2}\right) \\ \sin\left(\theta_k + \frac{u_k(2)}{2}\right) + \frac{u_k(1)}{D}\cos\left(\theta_k + \frac{u_k(2)}{2}\right) & \sin\left(\theta_k + \frac{u_k(2)}{2}\right) - \frac{u_k(1)}{D}\cos\left(\theta_k + \frac{u_k(2)}{2}\right) \\ \frac{2}{D} & \frac{2}{D} \end{bmatrix} \tag{23}$$

Since all of the model error in equation (20) is expressed by $G_k\mathbf{W}$, the process covariance matrix is expressed by

$$Q_k = \mathrm{cov}(G_k\mathbf{W}) = G_k\,\mathrm{cov}(\mathbf{W})G_k^T \tag{24}$$

where

$$\mathrm{cov}(\mathbf{W}) = \begin{bmatrix} \sigma_r^2 & 0 \\ 0 & \sigma_l^2 \end{bmatrix} \tag{25}$$

This matrix is a diagonal matrix owing to the assumption that the errors of the right and left wheels are independent.

For the measurement error we assume a white noise V with a covariance R. The value of R is determined by experiment. Based on that assumption, the measurement error model is given by

$$\gamma_j = h(\hat{\mathbf{X}}(k+1|k)) + R \tag{26}$$

The estimated position with the Kalman filter is expressed as [14]

$$\hat{\mathbf{X}}(k+1|k+1) = \hat{\mathbf{X}}(k+1|k) + \mathbf{K}(k+1)(\gamma_j(k+1) - \hat{\gamma}_j(k+1|k)) \tag{27}$$

The discrete nonlinear Kalman filter gains are determined by

$$\mathbf{K}(k+1) = \frac{P(k+1|k)H_x^T}{S(k+1)} \tag{28}$$

where H_x is the Jacobian of the measurement function h (equation (13)) given by

$$H_x = \begin{bmatrix} \dfrac{R_j(2) - X(2)}{\Delta} \\ \dfrac{R_j(1) - X(2)}{\Delta} \\ \dfrac{(R_j(2) - X(2))^2 + (R_j(1) - X(1))^2}{\Delta} \end{bmatrix} \tag{29}$$

$$\Delta = ((R_j(1) - X(1))\cos(q_k) + (R_j(2) - X(2))\sin(q_k))^2 + ((R_j(2) - X(2))\cos(q_k) + (R_j(1) - X(1))\sin(q_k))^2$$

$P(k+1|k)$ is the predicted covariance matrix of the process at the discrete time $(k+1)$ and given by

$$P(k+1|k) = F_x P(k|k) F_x^T + Q_k \tag{30}$$

$P(k|k)$ is the process covariance matrix at discrete time k, and F_x is the Jacobian of the process function f given by

$$F_x = \begin{bmatrix} 1 & 0 & -u_k(1)\sin\left(\vartheta + \dfrac{u_k(2)}{2}\right) \\ 0 & 1 & u_k(1)\cos\left(\vartheta + \dfrac{u_k(2)}{2}\right) \\ 0 & 0 & 1 \end{bmatrix} \tag{31}$$

$S(k+1)$ is the predicted measurement covariance given by

$$S(k+1) = H_x P(k+1|k) H_x^T + R \tag{32}$$

The update of the covariance matrix is performed by

$$P(k+1|k+1) = P(k+1|k) - \mathbf{K}(k+1) S(k+1) \mathbf{K}(k+1)^T \tag{33}$$

4. Simulation Results

This section presents simulation results of the system performance. In the first experiment the system performance is tested for motion along a straight path of 8 m. Average travel speed is 0.6 m s^{-1}, 8 reflectors are used, and measurement frequency is 5 Hz. Figure 7 shows the offset of the position estimate of the odometry model, compared with the offset determined by the Kalman filter. As shown (and expected), the offset of the odometry estimate increases as time (and distance) increases, while the offset with the Kalman filter is bounded to less than 1 cm. The error with the odometry estimate reaches a total lateral error of more than 0.2 m and 0.07 rad in the orientation, while the estimated lateral position error with the filter is less than 0.01 m (1 cm) and less than 0.02 rad.

For the second experiment, an external disturbance is introduced to each wheel for 0.2 s (Fig. 8). During the disturbance, the lateral position estimate increases to 0.2 m and the orientation error is increased to 0.05 rad. The Kalman filter reduces these errors to a minimal value after 2 s.

Finally, the system response to an initial error in position estimation is tested. In the first experiment, an initial lateral offset of 10 cm is presented (both in X and Y). As shown in Fig. 9, the error is damped, and after 3 s, the position estimate returns to its nominal value. An interesting phenomena occurs with the estimate of the angular estimate. Although no initial error is introduced to the orientation, the lateral position error

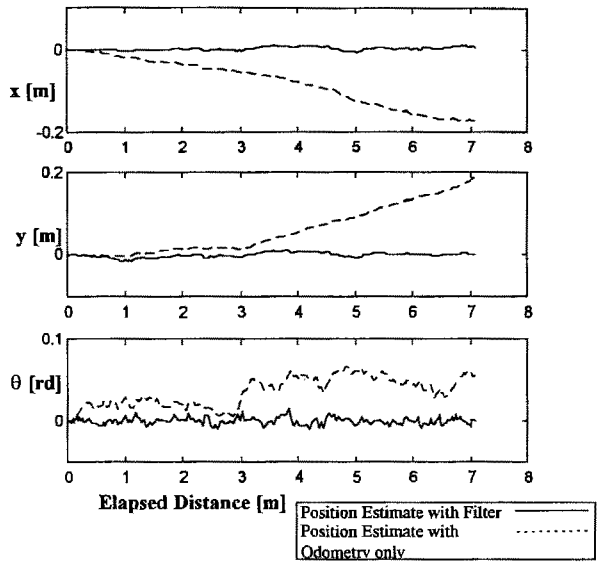

Fig. 7. The offset of the position estimate of the Odometry model compared with the offset determined by the Kalman filter.

affects the orientation estimate. This is due to the nature of the Kalman filter which "compares" the estimate angular measurement of the reflectors to the actual measurement. Initially, the filter detects a large deviation between the two measurements, but the cause of that deviation can be related both to lateral or angular error. However, after 1 s the filter detects the source of the deviation, and the angular error is rapidly corrected.

Figure 10 shows the filter's response to an initial angular error of 0.1 rad (5.6°) and no lateral position errors. As shown, the angular error is rapidly damped in less than 0.2 s, compared with 3 s for damping the lateral error. The reason for that is similar to that of the sensitivity of the filter to angular measurement as shown in the previous experiment. Each angular measurement is compared to the predicted measurement, and

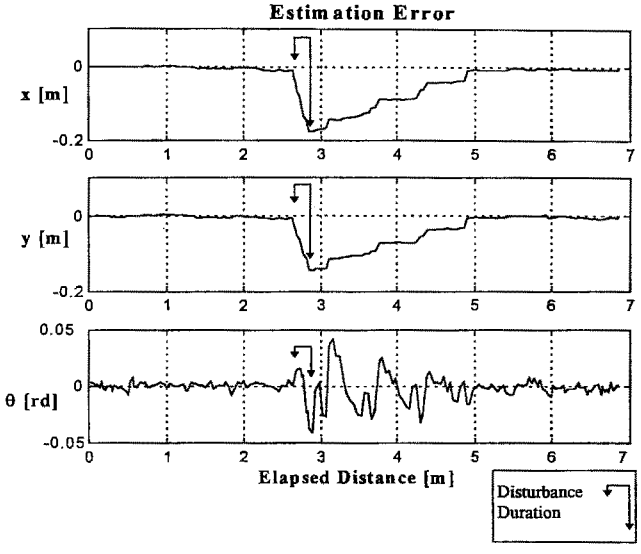

Fig. 8. Effects of introducing an external disturbance.

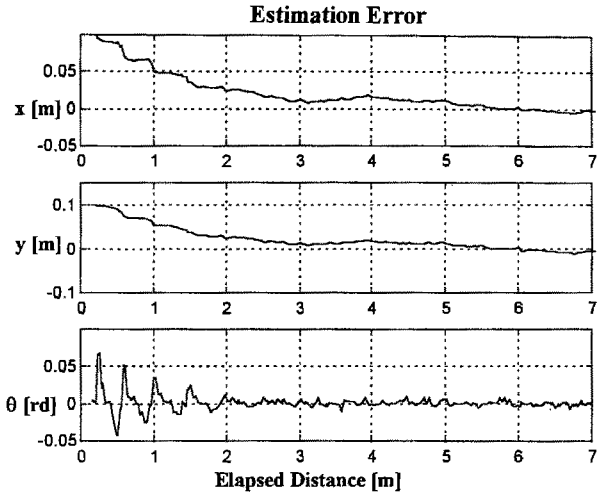

Fig. 9.

any deviation is immediately detected and processed by the filter. In the case of a lateral error, the filter requires several iterations to process these measurements and correct the lateral error, but only a few measurements are required to correct the angular errors.

5. Sensitivity of the Kalman Filter to the Process Parameters

5.1 Sensitivity to Vehicle Speed

In this experiment the filter sensitivity to the vehicle speed is tested. The vehicle travels several times along a predetermined path, each time at a different speed. In each test, the average errors are recorded. Figure 11 shows the results of this experiment. As shown, there is a clear relation between the vehicle speed and estimated position error. These results are as expected, because when the speed increases, the vehicle travels

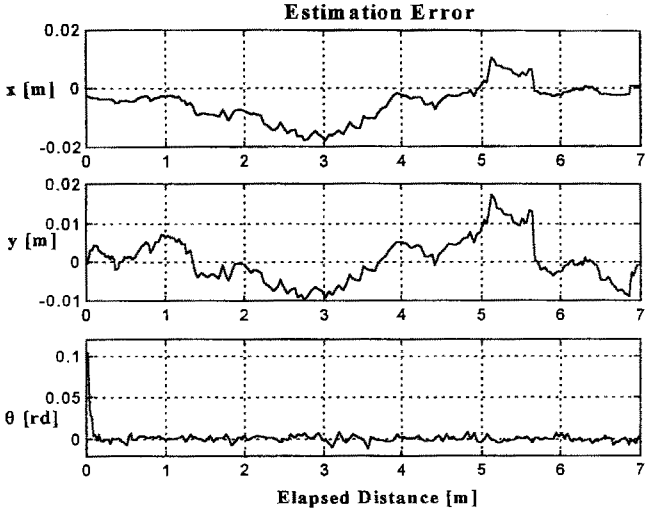

Fig. 10.

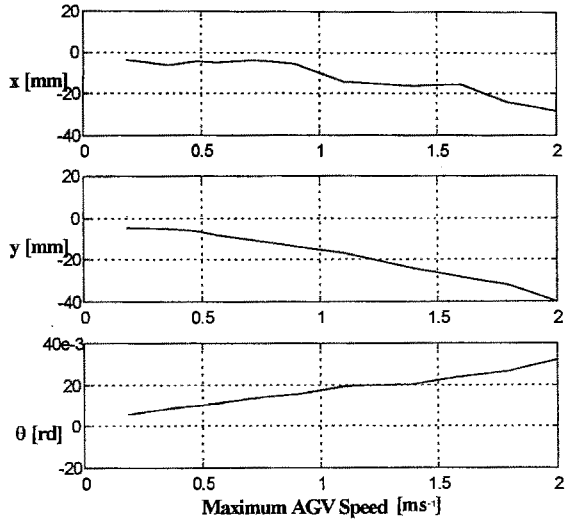

Fig. 11.

a larger "blind" distance, where it does not perform angular measurement, resulting in increased errors. It should be noted that during all these tests, the angular measurement frequency is kept constant at 5 Hz.

5.2 Sensitivity to Number of Landmarks

The number of landmarks used by the filter is important for several reasons:

As the vehicle is required to operate in an unstructured environment, it is expected that some of the landmarks will not be seen from each position, or will be out of the sensor's detection range.

The cost of setting up the positioning system can be reduced by decreasing the number of designated landmarks (initial cost includes, in addition to the hardware cost, the set-up cost, and accurate measurement of the landmark absolute position).

Figure 12 shows the average position error as a function of the number of landmarks used by the filter. In all experiments,

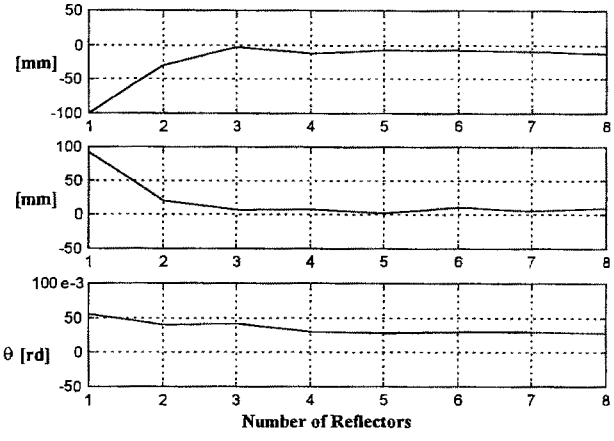

Fig. 12.

the measurement frequency is constant (5 Hz) and the travel path is identical, to eliminate the effect of parameters other than the number of landmarks. As shown in the figure, the effect is significant when there are fewer than 3 landmarks, mainly on the lateral position, and marginally on the angular position. Above 3 landmarks, there is no effect on the estimate position (lateral and angular). This can be explained by the direct relation between the measurement and the angular error, even for a single landmark. However, the filter can estimate lateral errors only after several measurements, optimally to three different landmarks. Similar results are shown in the experiment with different initial errors (Figs 9 and 10), where angular errors are detected instantaneously, while lateral errors require several measurements and almost 3 s to recover.

5.3 Sensitivity to Beacon Layout

Finally, the effect of landmark layout is presented. In this experiment, the vehicle is travelling along a straight path, with beacons positioned on several locations along the path. Figure 13 shows the lateral error (deviation) from the 4 m straight path. As shown, there are clear areas where the lateral error is higher than the nominal error.

Analysis of these areas shows that the increase in lateral errors occurs when the landmarks are in a close geometrical relationship to the vehicle. The close geometries are when two (or more) landmarks and the vehicle are located on one line, or when the lateral error is along the line between the vehicle and the landmarks. This can be explained as follows: if the lateral error is along the measurement line, the predicted angular measurement is identical to the actual measurement. The filter, therefore, cannot detect the lateral error, and only after several cycles (when the difference between the estimated and actual measurement is significant) does it correct the position estimate.

6. Conclusions

The implementation of a Kalman filter for data fusion in the positioning of an autonomous vehicle with several sensors is presented. The filter gains are adjusted according to a statistical analysis of the sensors' measurements, and the process model.

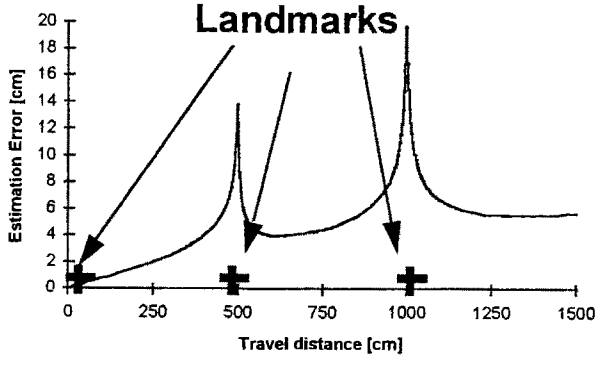

Fig. 13. Deviation from the straight path.

Simulation results of the filter's performance under various conditions show a better response to position errors in orientation than to lateral errors. However, the filter can detect and correct position errors (lateral and angular) and disturbances of 15 cm in less than 3 s. Sensitivity analysis of the filter for various vehicle speeds, shows that error increases linearly with speed. Also, it is shown that measurements to at least three landmarks are required, and the layout of these landmarks can affect the accuracy of the estimate. Based on these results, travel speed and landmark layout can be determined according to the process specifications and the sensors used by the filter.

References

1. M. Pietru, "Automated guided vehicle with absolute encoded guide-path", *IEEE Transactions on Robotics and Automation*, **7**(4), pp. 562–565, August 1991.
2. B. Evans (ed.), *AGV's Begin to Leave the Beaten Paths*, Mechanical Engineering, November 1988.
3. Denning Branch International Robotics, "Putting your ideas in motion", Company profile, 1995.
4. Nomad Technologies Inc., "Nomad 200 – Merging Mind and Motion", Product brochure, 1995.
5. K. Fujiwara, Y. Kawashima, H. Kato and M. Watanabe, "Development of a guideless robot vehicle", *Proceedings of the 11th International Symposium on Industrial Robots*, October 1981.
6. E. Nakano, N. Koyachi, Y. Agari and S. Hirooka, "Sensor system of a guideless autonomous vehicle in a flexible manufacturing system", *Proceedings of the 15th International Symposium on Industrial Robots*, October 1985.
7. B. Barshan, and H. F. Durrant-Whyte, "Inertial navigation system for a mobile robot", *Proceedings of the 1993 International Conference on Intelligent Robots and Systems*, pp. 2243–2248, 1993.
8. M. Ishikawa and M. Sampei, "State estimation of non-honolomic mobile robots using nonlinear observers", *IEEE International Conference on Robotic and Automation*, pp. 1379–1384, 1995.
9. M. Ishikawa and M. Sampei, "State estimation of mobile robot using non-linear observers", *Proceedings of the 23rd SICE Symposium on Control Theory*, pp. 297–300, Japan, 1994.
10. M. Ishikawa and M. Sampei, "State estimation of mobile robot using non-linear observers", *Proceedings of JSME Annual Conference on Robotics and Mechatronichs '94*, pp. 53–58, Japan, 1994.
11. M. Ishikawa and M. Sampei, "Nonlinear control of an autonomous mobile robot using non-linear observers", *Proceedings of '94 Korean Automatic Control Conference*, pp. 400–404, Korea, 1994.
12. Y. Bar-Shalom and T. E. Fortman, *Tracking and Data Association*, New York, Academic, 1988.
13. R. Smith, M. Self and P. Cheeseman, "Estimating uncertain spatial relationship in robotics", In I. Cox and J. Wilfong (eds), *Autonomous Robot Vehicles*, Springer-Verlag, New York, 1990.
14. J. J. Leonard and H. F. Durrant-Whyte, "Directed sonar sensing for mobile robot navigation", Kluwer Academic Publishers, 1992.
15. H.-J. von der Hardt, P. Arnould, D. Wolf and M. Dufant, "A method of mobile robot localization by fusion of odometric and magnetometric data", *International Journal of Advanced Manufacture Technology*, pp. 65–69, 1994.
16. D. J. Kriegman, E. Triendl and T. O. Binford, "Stereo vision and navigation in buildings for mobile robots", *IEEE Transactions on Robotics and Automation*, **5**(6), pp. 792–803, December 1989.
17. E. Stella, G. Cicirelli, F. P. Lovergine and A. Distante, "Position estimation for a mobile robot using data fusion", *Proceedings of the 10th IEEE International Symposium on Intelligent Control, Piscataway, NJ, USA* 95CB35815, pp. 565–570, 1995.
18. M. Huber, C. R. Bidlack, D. Kortenkamp, K. Mangis, D. Baker, A. S. Wu and T. E. Weymouth, "Computer vision for Carmel", *Proceedings of SPIE – The International Society for Optical Engineering*, **1831**, pp. 144–155, 1993.

19. Z. Katz and J. Asbury, "On-line position recognition for autonomous AGV navigational systems", *Journal of Manufacturing Systems,* **12**(2), pp. 146–152, 1993.
20. U. Wiklund, U. Andersson and K. Hyyppa, "AGV navigation by angle measurements", *Proceedings of the 6th International Conference on Automated Guided Vehicle Systems*, pp. 199–212, October 1988.
21. T. Nishizawa, A. Ohya and S. Yuta, "An implementation of on-board position estimation for a mobile robot", *IEEE International Conference on Robotics and Automation*, pp. 395–400, 1995.
22. S. Shoval, I. Zaietun and E. Lenz. "Layout of beacons for triangulation of AGV's in industrial environment", *Proceedings of the 13th International Conference on Production Research, Jerusalem, Israel,* pp. 485–488, August 1995.
23. D. A. Cicci, "Adaptive extended Kalman filter for angles-only tracking/intercept problems", *Journal of the Astronautical Sciences,* **41**(3), pp. 411–435, July–September 1993.
24. P. Moutarlier and R. Chatila, "An experimental system for incremental environment modelling by an autonomous mobile robot", *Experimental Robotics I, the First International Symposium*, pp. 327–346, June 1989.